Spin alignment following inelastic scattering of ^{17}Ne, lifetime of ^{16}F, and its constraint on the continuum coupling strength

R. J. Charity, K. W. Brown, J. Okołowicz, M. Płoszajczak, J. M. Elson, W. Reviol, L. G. Sobotka, W. W. Buhro, Z. Chajecki, W. G. Lynch, J. Manfredi, R. Shane, R. H. Showalter, M. B. Tsang, D. Weisshaar, J. R. Winkelbauer, S. Bedoor, and A. H. Wuosmaa

Phys. Rev. C **97**, 054318 — Published 16 May 2018

DOI: 10.1103/PhysRevC.97.054318

Spin alignment following the inelastic scattering of ^{17}Ne, the lifetime of ^{16}F, and its constraint on the continuum coupling strength

R.J. Charity,[1] K.W. Brown,[1,*] J. Okołowicz,[2] , M. Płoszajczak,[3] J.M. Elson,[1] W. Reviol,[1] L.G. Sobotka,[1] W.W. Buhro,[4] Z. Chajecki,[4] W.G. Lynch,[4] J. Manfredi,[4] R. Shane,[4] R.H. Showalter,[4] M.B. Tsang,[4] D. Weisshaar,[4] J.R. Winkelbauer,[4] S. Bedoor,[5] and A.H. Wuosmaa[5,6]

[1]*Department of Chemistry, Washington University, St. Louis, Missouri 63130, USA*
[2]*Institute of Nuclear Physics, Polish Academy of Sciences, Radzikowskiego 152, PL-31342 Kraków, Poland*
[3]*Grand Accélérateur National d'Ions Lourds (GANIL), CEA/DSM - CNRS/IN2P3, BP 55027, F-14076 Caen Cedex, France*
[4]*National Superconducting Cyclotron Laboratory and Department of Physics and Astronomy, Michigan State University, East Lansing, MI 48824, USA*
[5]*Department of Physics, Western Michigan University, Kalamazoo, Michigan 49008, USA*
[6]*Department of Physics, University of Connecticut, Storrs, Connecticut 06269, USA*

The sequential two-proton decay of the second excited state in ^{17}Ne, produced by inelastic excitation at intermediate energy, is studied. This state is found to be highly spin aligned, providing another example of a recently discovered alignment mechanism. The fortuitous condition that the second decay step is slightly more energetic than the first, permits the lifetime of the one-proton daughter, the ground-state of ^{16}F, to be determined from the magnitude of the final-state interactions between the protons. This new method gave a consistent result [Γ=20.6(57) keV] to that obtained by directly measuring the width of the state [Γ=21.3(51) keV]. This width allows one to determine the continuum coupling constant in this mass region. Real-energy continuum-shell-model studies yield a satisfactory description of both spectra and widths of low-energy resonances in ^{16}F and suggest an unusual large ratio of proton-proton to proton-neutron continuum couplings in the vicinity of the proton drip line.

I. INTRODUCTION

Studies of exotic nuclei close to drip lines is at the forefront of research in modern nuclear physics. These nuclei exhibit unusual features which have to be comprehended in a broader theoretical framework provided by an open-quantum-system approach. The foundation of nuclear-structure theory was provided by the interacting shell model (SM) [1, 2] which in its traditional form describes a nucleus as a closed quantum system where nucleons, in localized single-particle orbits, are isolated from the environment of the scattering states and decay channels. In the long term, this unfortunate separation between the discrete states and the continuum hindered a deeper understanding of nuclear properties. This is particularly obvious in exotic nuclei where reaction thresholds appear at low energies, and the impact of resonances and the nonresonant scattering continuum on nuclear properties is crucial. In this case, a unified theoretical framework which allows for a symmetric treatment of single-particle bound and scattering states in the many-body wave function becomes unavoidable. The attempts to reconcile the SM with nuclear reactions has given a push for the formulation of the real-energy continuum shell model (CSM) in a Hilbert space [3–6]. The alternative rigged-Hilbert-space-based description of many-body scattering states, resonances and bound states has lead to the development of complex-energy CSM, the so-called Gamow shell model [7–9].

Progress in the SM description of atomic nuclei has been achieved thanks to the understanding of basic properties of the nucleon-nucleon interaction and long-term efforts to develop effective interactions in different valence spaces. In this quest, light nuclei have traditionally been the testing ground of the SM, providing precise data on energy levels, electromagnetic transitions, nuclear moments, and various particle decays. With the progress in radioactive-beam experiments and the development of new theoretical approaches to reliably calculate properties of exotic nuclei with low-energy reaction thresholds, light nuclei still remain the favorite laboratory for testing nuclear interactions and many-body approaches.

The challenge for theory is to develop effective interactions in the extended space of configurations involving discrete states, resonances and the scattering continuum. In the recent version of the real-energy CSM, the shell model embedded in the continuum (SMEC) [5, 6, 10] which is employed in this work, the Hamiltonian is split into the monopole-based SM interaction in the subspace of localized single-particle states, and the Wigner-Bartlett interaction which couples nucleons in discrete and continuum states. The coupling strength and the spin-isospin exchange parameter of the Wigner-Bartlett interaction have to be determined by comparing SMEC results with the data concerning either the properties of resonances or the reaction observables. In this context, the spectroscopy of ^{16}F is of considerable interest due to the rearrangement of low-lying levels as compared to its mirror ^{16}N [Fig. 1(a)]. Due to their strong

* Present Address: National Superconducting Cyclotron Laboratory, Michigan State University, East Lansing, MI 48824, USA

$1s_{1/2}$ proton character, the J^π=0^-_1 and 1^-_1 states, the 2$^{\rm nd}$ and 3$^{\rm rd}$ excited states in ^{16}N, become the ground and 1$^{\rm st}$ excited states in ^{16}F. In this work, we will consider the changed ordering of levels in ^{16}N and ^{16}F, and describe the decay width of low-lying resonances in ^{16}F in the SMEC. The experimental width of these resonances allows one to extract the coupling strength and the spin-isospin exchange parameter of the Wigner-Bartlett continuum-coupling interaction in a nucleus beyond the proton drip line, at the interface between p and sd shells. In this analysis we shall use the precise information on the ground state width of ^{16}F which is determined in this work using a novel technique based on the sequential two-proton decay of an excited state in ^{17}Ne. We will also highlight the theoretical issue of the continuum coupling between like and unlike nucleons in the neighborhood of the drip line.

Recent studies have shown that light α-cluster nuclei (^{6,7}Li and ^{7}Be) inelastically excited in intermediate-energy collisions can have a very strong spin-alignment [11, 12]. Such spin alignments may be useful for measuring g factors of isomeric states. Hoff et al. [12] suggested an alignment mechanism for when the target nucleus is not excited which is quite general and independent of the structure of these light nuclei. To the extent that the spin-orbit and spin-spin interactions contribute little to the alignment, then the increased spin of the projectile must be compensated by a change in the reaction orbital angular momentum $\boldsymbol{L}$. From considerations of classical peripheral trajectories, one can find a matching energy where the dissipated kinetic energy required to promote the projectile to its excited state causes a reduction in the magnitude of $\boldsymbol{L}$ by the amount needed to increase the spin of the projectile to its excited-state value. Below this matching energy, the increased spin of the projectile comes from a reduction in the magnitude $\boldsymbol{L}$ and hence the final spin vector should be aligned close to direction of $\boldsymbol{L}$, i.e., perpendicular to the beam axis. On the other hand for energies well above the matching energy, these classical trajectories indicate that the change in the magnitude of $\boldsymbol{L}$ is much less than unity, and thus, in the quantum world, one expects a large probability that the magnitude of $\boldsymbol{L}$ is constant. Thus in order to conserve angular momentum, the orientation of $\boldsymbol{L}$ must undergo a small tilt, and thus the alignment of the excited state is perpendicular to $\boldsymbol{L}$. To test the generality of these ideas, it is important to observe such alignments for heavier non-α-cluster nuclei.

Two-proton emitters are a subject of great interest [13, 14]. The simplest type of two-proton emission is sequential decay where the emission of the first proton leaves the system in a long-lived intermediate state, which subsequently emits another proton. If this second proton has higher energy than the first, then it can catch up to this proton and then the two protons can interact via their repulsive Coulomb interaction. Such interactions can suppress events with small relative angles between the protons giving sensitivity to the lifetime of the intermediate state. This is similar to studies of hot nuclear systems where small-angle correlations between particles were used to infer the space-time extent of their source [15–17].

All of these phenomena can be studied using the inelastic excitation of ^{17}Ne projectiles to their 2$^{\rm nd}$ excited state. This excitation involves no change in parity and increases the spin by two units [Fig. 1(b)], similar to the ^{6,7}Li and ^{7}Be studies, and so should be a good test of the generality of the alignment mechanism. This state has been shown to undergo sequential two-proton decay through the ^{16}F$_{g.s.}$ resonance by Brown *et al.* [18]. In this paper we extend the analysis of the data from Brown *et al.* focusing on the alignment of the excited-state spin vector and the lifetime of ^{16}F$_{g.s.}$.

II. EXPERIMENTAL METHODS

The experiment was performed at the Coupled Cyclotron Facility at the National Superconducting Cyclotron Laboratory at Michigan State University. Details have been published elsewhere [18–20]. Briefly, a mixed ^{17}Ne(E/A=62.9 MeV, 11%, 1.6×10^4 pps)-^{15}O(E/A=52.1 MeV, 89%) secondary beam was produced from a primary ^{16}O beam (E/A=150 MeV, 175 pnA). This secondary beam impinged on a 1-mm-thick ^{9}Be target and charged particles produced in the subsequent reactions were detected in the High Resolution Array (HiRA) [21] whose fourteen E-ΔE telescopes were arranged around the beam axis and subtended polar angles from 2° to 13.9°.

The CsI(Tl) E detectors in each telescope were calibrated using beams of E/A=55 and 75 MeV protons and E/A=73 and 93 MeV ^{14}O. The ^{14}O calibration was used for ^{15}O fragments with a small modification determined from elastically-scattered ^{15}O beam particles that were detected in the most forward angle telescopes. The relative locations of the target and each HiRA telescope were determined accurately using a coordinate measurement machine.

III. EXPERIMENTAL RESULTS

The detected ^{17}Ne* $\rightarrow 2p+^{15}$O events were produced only from the ^{17}Ne component of the beam as verified from their reconstructed center-of-mass velocity which were similar to the higher ^{17}Ne beam velocity. The excitation-energy spectrum of ^{17}Ne fragments obtained from $2p+^{15}$O events has been described in [20]. Figure 2(a) shows this spectrum (circles) only in the vicinity of the peak associated with the 2$^{\rm nd}$ excited state. The equivalent spectrum for events where the ^{15}O fragment is emitted transversely from the ^{17}Ne* parent is shown by the squares. This gives improved E^* resolution as the uncertainty of the ^{15}O velocity due to its large energy loss in the thick target acts only in second order.

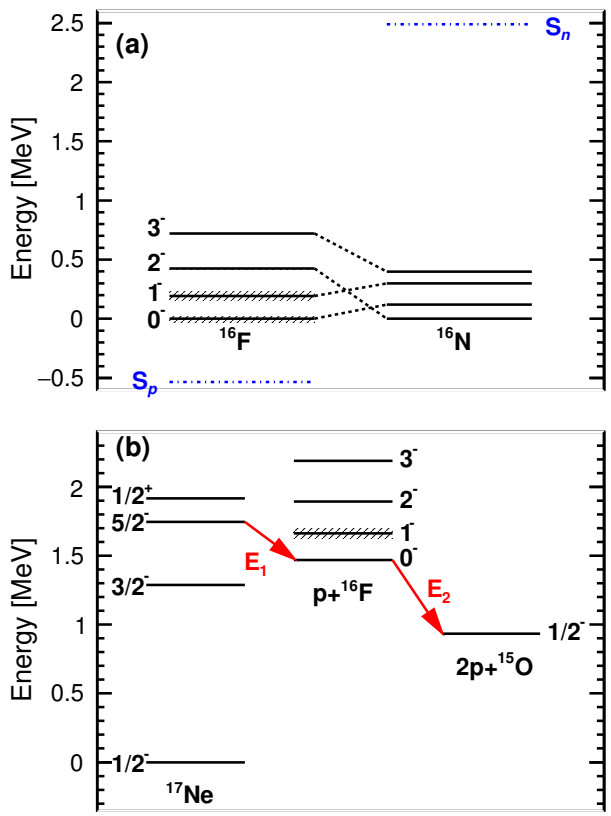

FIG. 1. (a) Comparison of the ordering of the low-lying levels in the mirror nuclei: ^{17}F and ^{16}N and their respective nucleon-decay thresholds. (b) Compilation of low-lying states in ^{17}Ne, ^{16}F, and ^{15}O used to illustrate the sequential $2p$ decay of the 2$^{\rm nd}$ excited state of ^{17}Ne.

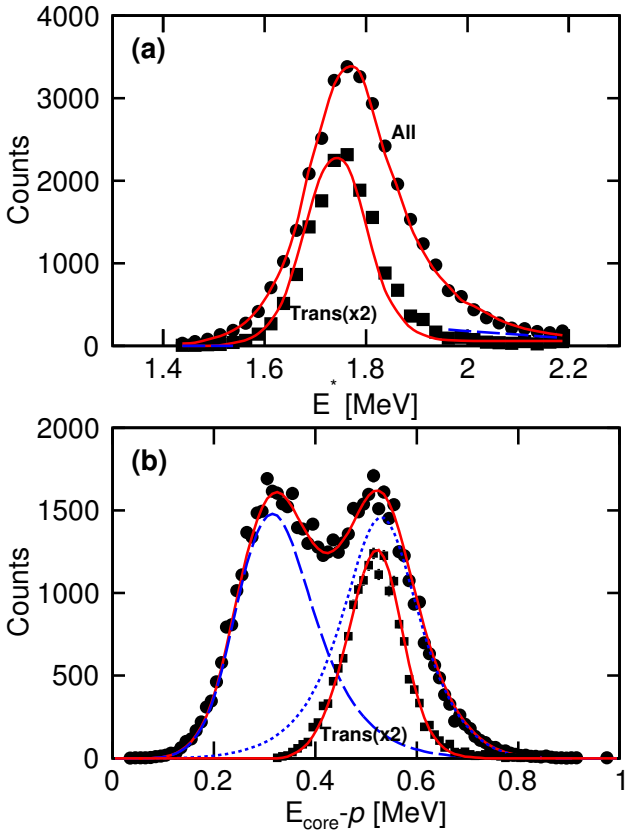

FIG. 2. (a) ^{17}Ne excitation-energy spectra reconstructed from detected $2p$+^{15}O events. Circles represent contributions from all ^{15}O C.M. emission angles ($\theta_{15}^{C.M.}$) while squares are for transverse emissions ($|\cos\theta_{15}^{C.M.}| < 0.4$). (b) p-^{15}O invariant-mass spectra for events from the decay of the ^{17}Ne 2$^{\rm nd}$ excited state. The circular data points were obtained from both emitted protons in each event, while the squares are for those protons identified as resulting from the decay of ^{16}F$_{g.s.}$ where the p-^{15}O decay axis is transverse to the beam axis. All solid curves are fits to the corresponding data. The dashed and dotted curves show the simulated decomposition of the first spectrum into its contributions from the first and second emitted proton, respectively.

The intrinsic width of this state is expected to be very small (0.23 eV [22]) and thus the observed widths of the spectra in Fig. 2(a) represent the experimental resolution. An accurate determination of this resolution is important for extracting the width of the ^{16}F intermediate state. The curves in Fig. 2 are the results of Monte Carlo simulations of sequential decay incorporating the experimental acceptance and resolution of the detectors [18]. The energy resolution (from energy-loss in the target and CsI(Tl) resolution) and angular resolution (from multiple scattering in the target) incorporated in these simulations have been fine tuned to best reproduce the measured spectra. The fitted centroid has an excitation energy of 1.745(7) MeV and a total decay energy of E_T=0.812(7) MeV.

The invariant-mass distribution for each p-^{15}O pair in $2p$+^{15}O events associated with the 2$^{\rm nd}$ excited state is plotted in Fig. 2(b) by the circular data points. As shown in Ref. [18], the higher-energy peak corresponds to the decay of the ground state of ^{16}F. We identify the first (second) decays, E$_1$ (E$_2$), with the lower (higher) energy proton. The same proton selection was applied to our simulated events and was found to lead to only an 11% level of misidentification. This can also be gauged from the overlap of the dotted and dashed curves in Fig. 2(b) that show the true decomposition of the fitted p-^{15}O invariant-mass spectrum into its contributions from each proton. To be consistent, we have kept these misidentified events when calculating the angular dependencies of the simulated efficiencies for detecting each proton which are used to correct the corresponding experimental distributions.

With the identification of the two protons, the invariant-mass spectra of ^{16}F can be reconstructed. The spectra indicated by the square data points in Fig. 2(b) show this distribution for events where the p-^{15}O decay axis is transverse to the beam axis (improved resolution). In the R-matrix theory of sequential decay [23], the distribution of the decay energy E_2 of the intermediate ^{16}F state is the product of a barrier penetration factor for the

emission of the first proton ($E_1 = E_T - E_2$, ℓ=2) and the profile function of the ^{16}F$_{g.s.}$ resonance that is defined by its resonance energy E_r and its reduced decay width γ^2. These quantities were obtained by fitting both distributions in Fig. 2(b) with our simulations. The fitted resonance energy is E_r=527(7) keV, consistent with the AME2016 tabulation [24] of 535.6(83) keV. For a channel radius of a=4.85 fm, we obtain γ^2=2.05(57) MeV giving a FWHM of the profile function of Γ=21.3(51) keV and $E_1 = E_T - E_r$=0.285(7) MeV.

A. Alignment

The angular distributions of the first and second proton relative to the beam axis in their respective center-of-mass systems (θ_{p_1} and θ_{p_2}) are shown in Figs. 3(b) and 3(c). These distributions have been corrected for the experimental efficiency as determined from our simulations. The angular distribution for the second proton is isotropic (flat) consistent with the expectation for decay from the ^{16}F$_{g.s.}$(J^π=0$^-$). The direction of the orbital angular momentum vector of the first proton must show strong alignment along the beam axis as it has a prominent peak at $\cos(\theta_{p_1}) = 0$. Such an alignment has been observed in the inelastic scattering of ^{6}Li, ^{7}Li and ^{7}Be projectiles [11, 12] when the target nucleus remains in it ground state. The excitation-energy distribution of the target nucleus determined using two-body kinematics with the deduced ^{17}Ne* momentum is shown in Fig. 3(a). There is a large peak at E^*_{target}=0 whose width is consistent with the experimental resolution as indicated by the dashed curve. Most of the yield is associated with this target "ground-state" peak and, to allow comparisons with the other alignment studies, the distribution in Fig. 3(b) has been gated on this peak.

To extract the magnetic-substate probability $p^\ell(m)$ of the decay orbital angular momentum, the angular distribution in Fig. 3(b) was fit with a sum of squared associated Legendre polynomials for ℓ=2. The fitted and individual components are indicated by the curves in Fig. 3(b). This probability distribution is shown by the circular data points in Fig. 4 where the expected symmetry $p^\ell(-m) = p^\ell(m)$ [11] is enforced. The magnetic substate distribution $p^J(m)$ of the spin vector $\boldsymbol{J}$ of the ^{17}Ne excited state can be determined from this distribution in a similar manner as in [11] where the two substate distributions are related via Clebsch-Gordan coefficients,

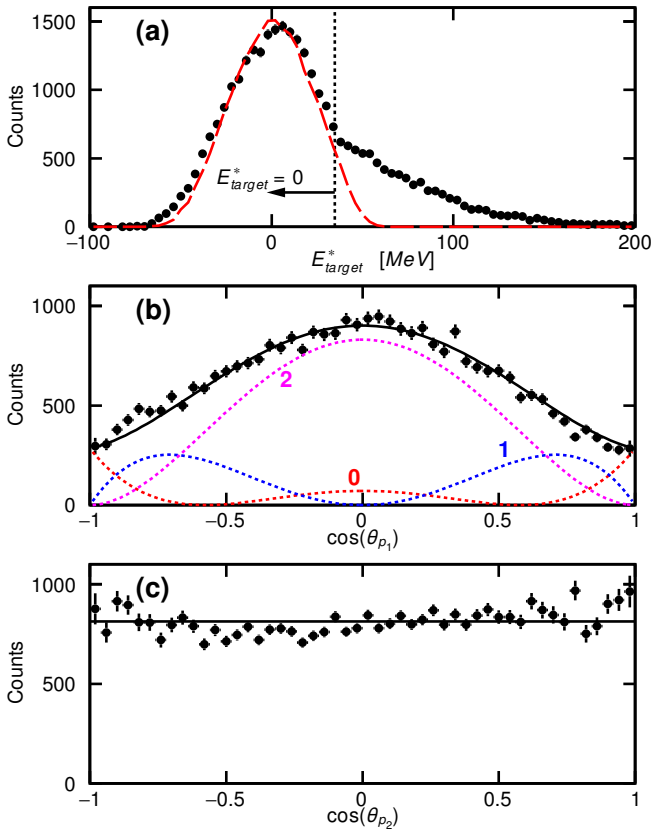

FIG. 3. (a) Excitation-energy distribution of the target nucleus for events which lead to the 2nd-excited state of ^{17}Ne. Data points are experimental values while the dashed curve is from our simulations with no target excitation. The gate used to select ground-state target events is indicated. (b) and (c) give the efficiency-corrected angular distributions of the first and second emitted protons relative to the beam axis. The solid curve in (a) shows a fit with a sum of squared associated Legendre polynomials (ℓ=2) with the individual components indicated by the dashed curves labeled with their m value. The data in (b) are consistent with a flat distribution (horizontal line).

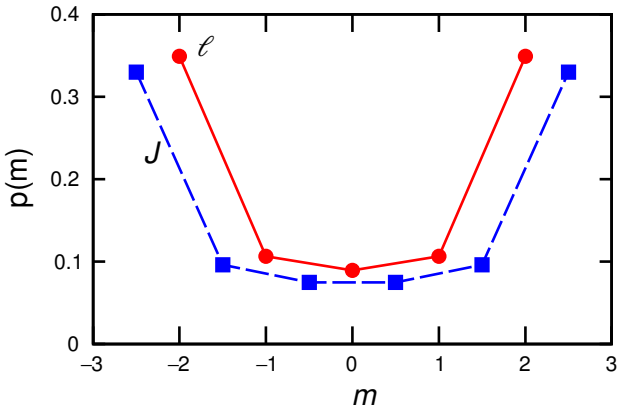

FIG. 4. Magnetic substate probability distributions extracted from the data. Circles correspond to the orbital angular momentum (ℓ) of the first emitted proton while the squares represent the spin (J) of the ^{17}Ne* fragment. Error bars are smaller than the data points.

i.e.,

$$
\begin{aligned}
m^{\ell}(2) &= \left\langle 2,2,\frac{1}{2},\frac{1}{2},\middle|\,\frac{5}{2},\frac{5}{2}\right\rangle^{2} m^{J}(5/2) \\
&+ \left\langle 2,2,\frac{1}{2},-\frac{1}{2}\middle|\,\frac{5}{2},\frac{3}{2}\right\rangle^{2} m^{J}(3/2), \\
m^{\ell}(1) &= \left\langle 2,1,\frac{1}{2},\frac{1}{2}\middle|\,\frac{5}{2},\frac{3}{2}\right\rangle^{2} m^{J}(3/2) \\
&+ \left\langle 2,1,\frac{1}{2},-\frac{1}{2}\middle|\,\frac{5}{2},\frac{1}{2}\right\rangle^{2} m^{J}(1/2), \\
m^{\ell}(0) &= \left\langle 2,0,\frac{1}{2},\frac{1}{2}\middle|\,\frac{5}{2},\frac{1}{2}\right\rangle^{2} m^{J}(1/2) \\
&+ \left\langle 2,0,\frac{1}{2},-\frac{1}{2}\middle|\,\frac{5}{2},-\frac{1}{2}\right\rangle^{2} m^{J}(1/2).
\end{aligned}
\tag{1}
$$

By solving these equations, we obtain the m^J distribution plotted in Fig. 4 as the square data points. The $|m| = J$ values, corresponding classically to the spin vector pointing parallel and antiparallel to the beam axis, are strongly populated as was found for the excitation of the cluster nuclei ^{6}Li, ^{7}Li, and ^{7}Be at similar values of E/A [11, 12]. The extent of the alignment can be characterized by the scaler:

$$
\mathcal{A} = \sum_{m} \frac{3m^2 - J(J+1)}{J(2J-1)} p^J(m) \tag{2}
$$

with $\mathcal{A}$=1(-1) corresponding to the largest alignment along (transverse) to the quantization axis. The alignment of the ^{17}Ne* spin vector is $\mathcal{A}$=0.51(1) which is strikingly similar to the values of 0.51(1), 0.49(1), 0.49(1) obtained with the ^{6}Li, ^{7}Li, and ^{7}Be projectiles, respectively. Our result demonstrates that this alignment mechanism is not just confined to lighter, α-cluster nuclei and supports the argument that large longitudinal alignments result from an angular-momentum-excitation-energy mismatch conditions, occurring above a threshold bombarding energy, a mechanism that is independent of the scattering potential and the nature of the excitation [12].

B. p-p Final-State Interactions

As the second proton has a larger kinetic energy than the first, if the two protons are emitted in the same direction, the second proton can catch up to the first. Using $\Gamma(^{16}\mathrm{F}_{g.s.})$=20 keV and assuming the second proton is emitted at one half life, then the two protons will be ∼700 fm away from the ^{15}O core when they are in close proximity. Noticeable defections of the proton trajectories will occur if they come within a few hundred fm of each other as their relative energy is only 17 keV (classical distance of closest approach is 85 fm). With this low relative energy, and large distances of action, the target's tidal Coulomb field and the short-ranged p-p spin-singlet force are negligible.

The efficiency-corrected θ_{pp} distribution is plotted in Fig. 5. The full distribution is shown in the inset while the region of smaller angles is shown in the main figure. This distribution is largely isotropic as expected given that the second proton is initially emitted isotropically. However for θ_{pp} <25° there is a suppression of the yield which can be attributed to these "catch-up" events. Surprisingly at 30° < θ_{pp} <60° there is also a small enhancement (∼10%) of events relative to those at larger θ_{pp}. With the final-state interactions moving events from small relative angles to intermediate values, one might expect to see an enhancement at these intermediate angles. Indeed one does observe such an effect in the predicted primary θ_{pp} distributions after final-state interactions are included in our simulations. However when the experimental resolution is added, this enhancement is completely washed out. Therefore we conclude that this enhancement in the data does not originate from the final-state interactions. Rather, it appears the second proton retains a memory of the emission direction of the first proton. Probably we are observing a much milder version of the decay correlations found for the first excited state (J^π=2^+_1) state in ^{16}Ne where the energies of the protons are consistent with sequential decay, but the θ_{pp} distribution is strongly enhanced for small relative angles [20]. Further experimental and theoretical efforts are needed to better understand this effect.

However in order to extract a lifetime, one must know the primary θ_{pp} distribution before the effect of the final-state interactions. We have assumed that this enhancement increases monotonically as $\theta_{pp} \rightarrow 0°$ and have taken

the smooth function

$$W(\cos\theta_{pp}) = a - \frac{b}{2}\frac{1-\exp(\frac{\cos\theta_{pp}-1}{d})}{1+\exp(\frac{\cos\theta_{pp}-1}{d})}, \qquad (3)$$

with three parameters (a, b, c) to model it. This function changes from a flat distribution at $\cos\theta_{pp} \sim$ -1 to a linear increase at $\cos\theta_{pp} \sim$1 which was able to reproduce the ^{16}Ne(J^π=2_1^+) data. The parameters a, b, c, can be determined from fitting from the experimental distribution for θ_{pp} >45° where the final-state interactions are minimal. We then use the extrapolated functional form to determine the magnitude of the final-state suppression at smaller angles.

For the final-state interaction, as both protons are far from the target nucleus when they interact, we randomly choose asymptotic classical proton-core trajectories with exit parameters (equivalent to impact parameters for entrance channels) consistent with the decay orbital angular momentum. Subsequently, the p-p hyperbolic orbits are calculated analytically. The details of these initial p-core trajectories were found to have little influence on the final result.

Fits with constrained values of Γ are shown in the main figure, while the best fit and the fitted primary distribution are shown in the inset by the solid and dashed curves, respectively. The fitted width is 23.3(30) keV, but it is dependent on the assumed parameterization of the primary distribution. To gauge the magnitude of this dependence, we have assumed an alternative primary distribution that becomes flat for $\cos\theta_{pp} > 0.6$. The fitted width now drops to Γ=17.4(25) keV. Using the difference of these two results to estimate the systematic error, we obtain Γ=20.6(57) keV which is very similar in mean and uncertainty with the value of Γ=21.3(51) keV obtained from fitting the invariant-mass peaks in Fig. 2(b). With the uncertainty in the shape of the primary distribution, our second method of extracting the width offers no advantages or disadvantages over measuring the widths directly. But in this case, these two independent methods provided identical values giving us great confidence in this result. Previous measurements of this quantity are consistent with our results [Fig. 6(a)].

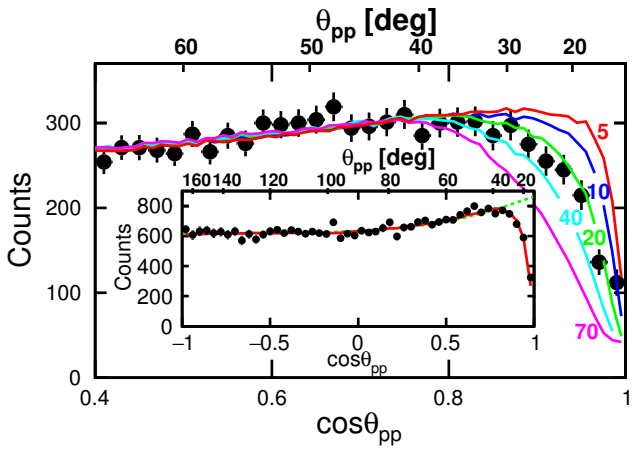

FIG. 5. Efficiency-corrected distribution of the relative angle θ_{pp} between the emission directions of the two protons in their respective center-of-mass frames. The full distribution is shown in the inset, while the main figure highlights the region of smaller relative angles. The curves are calculations incorporating final-state interactions between the two protons. These curves in the main figure are labeled by the width Γ of the ^{16}F$_{g.s.}$ resonance in keV. The solid curve in the inset is the best fit Γ=23.3 keV, while the fitted primary distribution before the inclusion of final-state interactions is shown as the dotted curve.

IV. CONTINUUM SHELL MODEL CALCULATIONS

Weakly-bound or unbound nuclei in the vicinity of drip lines provide great challenges for nuclear theory due to the impact of coupling to both the scattering continuum and the decay channels. The microscopic structure of many-body resonances can be considered in the SMEC [6, 10, 25–27] which is the recent realization of the open-quantum-system formulation of the shell model [10, 28]. The advantage of SMEC is that it allows one to also calculate reaction observables and, as such, provides a unified approach to nuclear structure and reactions. Here we wish to investigate if the widths for J^π=0_1^-, 1_1^-, 2_1^-, and 3_1^- resonances reported in a number of recent experiments can be explained by the SMEC calculation.

In the SMEC, the Hilbert space is divided into two orthogonal subspaces $\mathcal{Q}_0$ and $\mathcal{Q}_1$ containing 0 and 1 particles in the scattering continuum, respectively. An open-quantum-system description of the $\mathcal{Q}_0$ space includes couplings to the environment of the decay channels through the energy-dependent effective Hamiltonian: $\mathcal{H}(E) = H_{\mathcal{Q}_0\mathcal{Q}_0} + W_{\mathcal{Q}_0\mathcal{Q}_0}(E)$. Here $H_{\mathcal{Q}_0\mathcal{Q}_0}$ is the standard SM Hamiltonian, $W_{\mathcal{Q}_0\mathcal{Q}_0}(E) = H_{\mathcal{Q}_0\mathcal{Q}_1}G^{(+)}_{\mathcal{Q}_1}(E)H_{\mathcal{Q}_1\mathcal{Q}_0}$ is the energy-dependent continuum-coupling term, E is a scattering energy, $G^{(+)}_{\mathcal{Q}_1}(E)$ is the one-nucleon Green's function, and $H_{\mathcal{Q}_0,\mathcal{Q}_1}$, $H_{\mathcal{Q}_1\mathcal{Q}_0}$ are the coupling terms between $\mathcal{Q}_0$ and $\mathcal{Q}_1$. The zero of the energy scale is fixed at the lowest one-nucleon emission threshold. The one-nucleon decay channels are defined by the coupling of one nucleon in the continuum of nucleus A to SM eigenstates of an $(A-1)$ nucleus. The eigenvalues of the effective Hamiltonian $\mathcal{H}(E)$ are real at energies below all decay thresholds and complex above the lowest decay threshold.

The eigenstates $|\Psi_j\rangle$ of $\mathcal{H}(E)$ are the linear combinations of SM states $|\psi_i\rangle$, generated by the orthogonal transformation matrix $[b_{ji}(E)]$. Squared matrix elements $b^2_{ji}(E)$ are weights of the SM eigenstate $|\psi_i\rangle$ in the SMEC eigenstate $|\Psi_j\rangle$ at an energy E. The energies $E^{(j)}$ and widths $\Gamma^{(j)}$ of the resonance states are found by solving

the fixed-point equations:

$$E^{(j)} = \tilde{E}^{(j)}(E = E^{(j)})$$

and

$$\Gamma^{(j)} = \tilde{\Gamma}^{(j)}(E = E^{(j)})$$

where $\mathcal{E}^{(j)}(E) = \tilde{E}^{(j)}(E) + i\frac{\tilde{\Gamma}^{(j)}(E)}{2}$ are the (complex) eigenvalues of the effective Hamiltonian $\mathcal{H}(E)$. The continuum induced mixing of SM states is particularly strong if avoided crossings appear in the spectrum of SMEC eigenstates [10, 26, 27]. This mixing effect can be studied using the continuum-coupling correlation energy $E^{(j)}_{\rm corr}(E) = \langle\Psi_j|W_{\mathcal{Q}_0\mathcal{Q}_0}(E)|\Psi_j\rangle$ in the SMEC eigenstate Ψ_j. Above the particle-emission threshold ($E > 0$), the expectation value of the continuum coupling term $W_{\mathcal{Q}_0\mathcal{Q}_0}(E)$ is complex and, hence $E^{(j)}_{\rm corr}(E) = Re\left[\langle\Psi_j|W_{\mathcal{Q}_0\mathcal{Q}_0}(E)|\Psi_j\rangle\right]$. It has been shown in Refs. [21,22] that the mixing of SM states is strongest at the minimum of the correlation energy [26, 27], *i.e.* at the centroid of the opportunity energy window for a formation of the SMEC eigenstate with strong collectivization of its SM components. This state carries many features of the nearby decay channel. The position of the centroid is determined by an interplay between the competing forces of repulsion (Coulomb and centrifugal interaction) and attraction (the continuum coupling). Detailed discussion of this near-threshold phenomenon can be found in Refs. [21,22].

There are two kinds of operators in $W_{\mathcal{Q}_0\mathcal{Q}_0}(E)$: $\mathcal{O}^K_{\beta\delta} = \langle a^\dagger_\beta \tilde{a}_\delta\rangle^K$, and $\mathcal{R}^{j_\alpha}_{\gamma\delta(L)\beta} = \langle\ a^\dagger_\beta\langle\ \tilde{a}_\gamma\tilde{a}_\delta\rangle^L\rangle^{j_\alpha}$. The matrix elements of $\mathcal{O}$ are calculated between the states in the $(A-1)$-particle system and, hence, couple different decay channels. The operator $\mathcal{R}$ acts between different SM wave functions in the A- and $(A-1)$-particle systems, *i.e.,* is responsible for both the mixing of the SM wave functions in the nucleus A and the coupling between decay channels. One should stress that the width of a state is not simply related to the product of spectroscopic and penetration factors. Due to continuum couplings by the operator $\mathcal{R}$, one may have both a large width associated with a small spectroscopic factor, or vice versa.

The Hamiltonian of the SMEC consists of the monopole-based SM interaction (referred to as WBP− [29]) in the full *psd* model space plus the Wigner-Bartlett contact interaction, $V_{12} = V_0\left[\alpha + \beta P^\sigma_{12}\right]\delta\langle\mathbf{r_1} - \mathbf{r_2}\rangle$, for the coupling between SM states and the decay channels. Here P^σ_{12} is the spin-exchange operator and $\alpha + \beta = 1$. The coupling constants are $V_{nn} = V_{pp} = V_0(\alpha - \beta)$ and $V_{np} = V_0(\alpha + \beta)$ between like and unlike nucleons, respectively. No two-body Coulomb interaction is included in WBP−. Radial single-particle wave functions in $\mathcal{Q}_0$ and the scattering wave functions in $\mathcal{Q}_1$ are generated using a Woods-Saxon (WS) potential which includes spin-orbit and Coulomb parts. The radius and diffuseness parameters of the WS potential are $R_0 = 1.27A^{1/3}$ fm and $a = 0.67$ fm, respectively. The spin-orbit potential is $V_{\rm SO} = 6.4$ MeV, and the Coulomb part is calculated for a uniformly-charged sphere of radius R_0. The depth of the central part for protons (neutrons) is adjusted to yield the energy of the single-particle state involved in the lowest one-proton (one-neutron) decay channel equal to the one-proton (one-neutron) separation energy in the ground state of ^{16}F (^{16}N). The continuum-coupling term $W_{\mathcal{Q}_0\mathcal{Q}_0}(E)$ breaks the isospin conservation due to different radial functions for protons and neutrons, and different proton and neutron separation energies.

The WBP− interaction had not been tuned to reproduce the spectra of ^{16}N and ^{16}F [Fig. 1(a)]. The experimental ordering of levels in ^{16}N is obtained if the strongly attractive $T = 0$ matrix elements: $\langle 0p_{1/2}1s_{1/2}; J^\pi = 0^-|V|0p_{1/2}1s_{1/2}; J^\pi = 0^-\rangle$ and $\langle 0p_{1/2}0d_{5/2}; J^\pi = 2^-|V|0p_{1/2}0d_{5/2}; J^\pi = 2^-\rangle$ become less attractive by 500 keV and 300 keV, respectively, as compared to their original values in WBP−. This change of the two matrix elements implies a small modification of WBP− monopole terms $M^{T=0}(0p_{1/2}1s_{1/2})$ and $M^{T=0}(0p_{1/2}0d_{5/2})$ which become -2.985 MeV and -3.863 MeV, respectively, as compared to -3.11 MeV and -3.988 MeV in the original WBP− interaction [29]. In ^{16}F, in addition to this change of the $T = 0$ two-body matrix elements, one has to correct the splitting between $0p_{1/2}$ and $1s_{1/2}$ single-particle levels. This is achieved by making $M^{T=0}(0p_{1/2}1s_{1/2})$= -4.085 MeV, about 1.1 MeV more attractive than in the bound mirror.

The continuum-coupling constant V_0 and the parameters α, β of Wigner-Bartlett interaction have been adjusted to reproduce the ground-state width of ^{16}F. This width depends mainly on V_0 and is insensitive to the ratio of V_{pp}/V_{np}. It is also insensitive to the modification of the monopoles $M^{T=0}(0p_{1/2}1s_{1/2})$, $M^{T=0}(0p_{1/2}0d_{5/2})$, and does not depend on the diffuseness parameter of the WS potential generating the radial single-particle wave functions in $\mathcal{Q}_0$ and the scattering wave functions in $\mathcal{Q}_1$.

The width of the 2^-_1 resonance also has little sensitivity to V_{pp}/V_{np}. In Fig. 6(c) we show that the predicted width of this state, using our adjusted value V_0, reproduces the experimental data including the results of Lee *et al.* and Stefan *et al.* which have small error bars. Contrary to the 0^-_1 and 2^-_1 resonances, the widths of the 1^-_1 and 3^-_1 resonances depend on the ratio V_{pp}/V_{np}. Now in Fig. 6(b), a significant discrepancy appears between the predicted width of the 1^-_1 resonance for V_{pp}/V_{pn}=0.46 and all but one of the experimental values. To analyze this discrepancy, we have reproduced the width of the 1^-_1 [34] by adjusting the strength V_0 for different values of the ratio V_{pp}/V_{np}, and calculated the 1σ distance: $d = (\Gamma_{\rm th} - \Gamma_{\rm exp})/\sigma(\Gamma_{\rm exp})$, between experimental and theoretical value for the width of 0^-_1 resonance. One can see in Table I that the width of the 0^-_1 resonance becomes consistent with the width of 1^-_1 resonance [34] within 3σ if the ratio of continuum coupling strengths V_{pp}/V_{np} is close to 4, much larger than the standard value $\sim$1/2. However even in the limiting case $V_{pp}/V_{np} \to \infty$, d remains significant. But rather than judging the merits

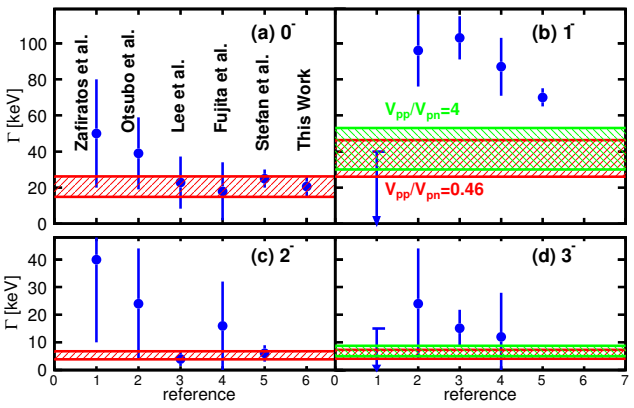

FIG. 6. (Color online) Measured widths of J^π=0^-_1, 1^-_1, 2^-_1, and 3^-_1 resonances in ^{16}F are compared with SMEC results. For the 1^-_1 and 3^-_1 states, predictions for both V_{pp}/V_{np}=0.46 and 4 are shown. The x axis references refers to previous experimental studies in time order of publication. The references are (1) Zafiratos *et al.* [30], (2) Otsubo *et al.* [31], (3) Lee *et al.* [32], (4) Fujita *el al.* [33], (5) Stefan *et al.* [34] and (6) this study. The lead authors of these studies are also identified in panel (a).

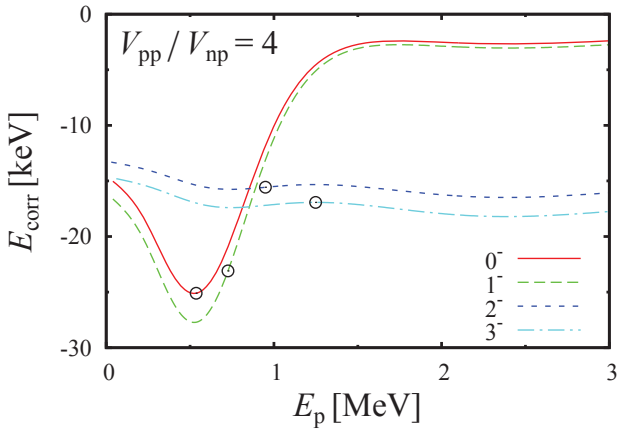

FIG. 7. (Color online) The continuum-coupling correlation energy in ^{16}F is plotted as a function of the proton energy E_p for the 0^-_1, 1^-_1, 2^-_1, and 3^-_1 resonances coupled to the elastic channel $[^{15}\mathrm{O}(1/2^-)\otimes\pi\ell_j]^{J^\pi}$. $E_p=0$ corresponds to the channel threshold. Open circles show E_{corr} for the 0^-, 1^-, 2^-, and 3^- resonances at their calculated energies. For more details, see the discussion in the text.

TABLE I. Distance in units of $\sigma(\Gamma_{\rm exp})$ between the calculated and measured width of 0^-_1 resonance for different values of V_{pp}/V_{np} and V_0 which reproduce the width of the 1^-_1 resonance reported by Stefan *et al.* [34].

V_{pp}/V_{np}	0.46	2	3	4	∞
d	3.96	3.21	3.07	2.93	2.63

on the calculations based on the small error bar of the measurement, we note the upper limit of the calculation is only 30% below the experimental value in Fig. 6(b). The strong enhancement of the ratio V_{pp}/V_{np} suggested by the analysis of these two independent measurements, is related to the resonance feature of $s_{1/2}$ proton single-particle orbits. A somewhat similar tendency has been found before in the studies of neutron separation energies in weakly-bound fluorine isotopes [35]. To reproduce the experimental binding systematics it was necessary to significantly increase the ratio of coupling constants V_{nn}/V_{np} in the proximity of the neutron drip-line, thus reducing the coupling between a proton in a well-bound orbit and a neutron in the scattering continuum.

The continuum-coupling correlation energy: $E^{(i)}_{\rm corr}(E)$, is a good indicator of the continuum-coupling induced collectivization as manifested by strong mixing of SM eigenstates in certain SMEC eigenstates. Figure 7 shows $E^{(i)}_{\rm corr}(E)$ for J^π=0^-_1, 1^-_1, 2^-_1, and 3^-_1 as a function of proton energy E_p above the elastic proton-decay threshold. Open circles show the correlation energies for these states at their calculated resonance energies. The parameters of the Wigner-Bartlett interaction are $V_{pp}/V_{np}=4$, $V_0=-8.77$ MeV fm^3. Using these values, one obtains: Γ =41.5 $\pm$ 11.5 keV for 1^-_1, 5.4 $^{+1.6}_{-1.4}$ keV for 2^-_1, and 6.9 $\pm$ 1.9 keV for 3^-_1 where the uncertainties reflect the uncertainty of V_0 constrained from the measured 0^-_1 width. One can see strong collectivization in the resonance doublet: 0^-_1 and 1^-_1. The calculated position of the 0^-_1 resonance is found at the centroid of the opportunity energy window for the continuum-coupling induced collectivization in the set of SM states. The 1^-_1 resonance is at the edge of its opportunity energy window and hence the collectivization of SM states in this resonance is weaker. The second doublet of resonances, 2^-_1 and 3^-_1, is unaffected by the coupling to the proton decay channel $[^{15}\mathrm{O}(1/2^-)\otimes\pi d_{5/2}]^{J^\pi}$.

Complex energy eigenvalues of the effective Hamiltonian above the particle-emission threshold depend on the energy E_p of a particle in the continuum. Figure 8 shows the widths functions for J^π=0^-_1, 1^-_1, 2^-_1, and 3^-_1 eigenvalues of the energy-dependent effective Hamiltonian $\mathcal{H}(E)$. Open circles indicate the value of the resonance width at the calculated resonance energy. One can see that the energy-dependent width functions for 0^-_1 and 1^-_1 states reach the maximum at $E_p\simeq 0.9$ MeV and decreases at higher proton energies in the continuum. Even at the maximum, the width of 1^-_1 state is smaller than the value reported by Stefan *et al.* [34]. On the contrary, widths functions for 2^-_1 and 3^-_1 resonances are growing monotonously in the whole range of considered proton energies ($E_p<3$ MeV).

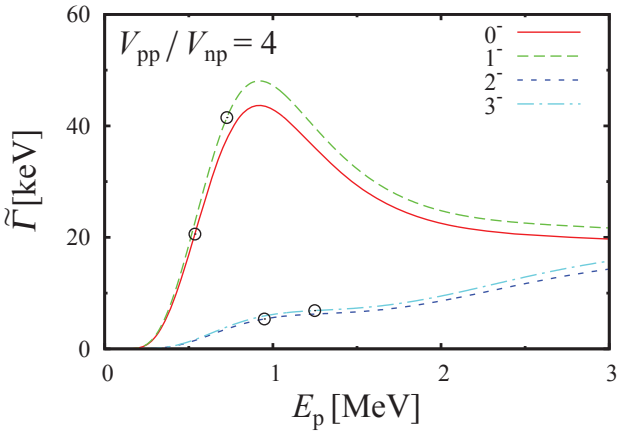

FIG. 8. (Color online) The width functions corresponding to 0_1^-, 1_1^-, 2_1^-, and 3_1^- eigenvalues of the effective Hamiltonian in ^{16}F. Open circles show the width of 0_1^-, 1_1^-, 2_1^-, and 3_1^- resonances at the resonance energies which follow from SMEC fixed-point equations. For more information, see the text.

V. CONCLUSIONS

In conclusion, we have observed the sequential two-proton decay of the J^π=5/2$^-$, 2$^{\rm nd}$ excited state of ^{17}Ne formed by inelastic scattering of ^{17}Ne beam particles off ^{9}Be target nuclei. When the target nucleus remains in its ground state, the spin vector of this excited state is highly aligned along the beam axis similar to that found for the excitation of lighter α-cluster nuclei. This result is consistent with the recently proposed alignment mechanism by Hoff *et al.* [12] which is independent of the detailed structure of the projectile and target and suggests many other examples will be found.

The decay width of ^{16}F$_{g.s.}$, the 1p daughter of the ^{17}Ne excited state, has been measured both from the width of its invariant-mass distribution and independently from the magnitude of final-state interactions between the two emitted protons. Both methods gave similar results: Γ=21.3(51) and 20.6(57) keV, respectively. The decay of low-energy ^{16}F states has been considered in the SMEC and the coupling interaction between the SM states and the scattering continuum has been constrained from our measured ground-state width. These studies indicate a strong reduction of the continuum coupling between the unbound proton and the well-bound neutron in ^{16}F resonances possibly due to the mismatch of radial wave functions for unlike nucleons.

This observation is in qualitative agreement with the analysis of Stefan *et al.* [34] who employed an extreme single-particle perspective and neglected the resonance features of ^{16}F. In a simple picture of ^{16}N (^{16}F) described as a core of ^{14}C (^{14}O) coupled to two neutrons (protons), it was concluded that the effective proton-neutron interaction in ^{16}F is strongly reduced and differ between mirror nuclei by as much as $\sim$ 40% [34]. The SMEC study gives a much more nuanced picture of the proton-neutron interaction in these mirror nuclei. Experimental energies of the 0_1^-, 1_1^-, 2_1^-, and 3_1^- levels in ^{16}N are well reproduced with only a slight adjustment of the $T = 0$ matrix elements $\langle 0p_{1/2}1s_{1/2}; J^\pi = 0^-|V|0p_{1/2}1s_{1/2}; J^\pi = 0^-\rangle$ and $\langle 0p_{1/2}0d_{5/2}; J^\pi = 2^-|V|0p_{1/2}0d_{5/2}; J^\pi = 2^-\rangle$ of the WBP$-$ interaction [29]. However, to obtain the correct spectrum in ^{16}F, the $M^{T=0}(0p_{1/2}1s_{1/2})$ monopole in $H_{\mathcal{Q}_0\mathcal{Q}_0}$ should be significantly more attractive. These monopole modifications have no significant affect on the lifetimes of the 0_1^-, 1_1^-, 2_1^-, and 3_1^- resonances. The predicted decay widths for the J^π=2_1^- and 3_1^- excited states are consistent with previous measurements, while the results for the J^π=1_1^- first-excited state is smaller than recent measurements. The ground-state width of ^{16}F determines the overall strength of the H_{Q_0,Q_1}, $H_{Q_1Q_0}$ coupling between SM states (in $\mathcal{Q}_0$) and the one-nucleon decay channels (in $\mathcal{Q}_1$) but is insensitive to the ratio of proton-proton V_{pp} and proton-neutron V_{pn} coupling constants. This ratio is constrained by the width of the 1_1^- resonance which suggests a significant reduction of the coupling between a proton in the continuum and a neutron in the well-bound single-particle state, hence the strong increase of the ratio V_{pp}/V_{pn} from its value found for nuclei near the valley of stability. This strong reduction of the continuum coupling matrix elements for unlike nucleons was also suggested in the analysis of the neutron separation energies in neutron-rich fluorine isotopes [35].

The correct treatment of the continuum is mandatory to understand the evolution of an effective nucleon-nucleon interaction from the valley of stability to the nucleon drip lines. In this task, light mirror nuclei provide an ideal laboratory to test the sensitivity of an effective interaction to different conditions of binding, and determine the coupling between nucleons in localized and continuum many-body states. However, further systematic experimental and theoretical efforts are needed in the future to obtain a reliable effective interaction for the open-quantum-system description of exotic properties of nuclei in different mass regions.

ACKNOWLEDGMENTS

This work was supported by the U.S. Department of Energy, Division of Nuclear Physics under grant No. DE-FG02-87ER-40316, No. DE-FG02-04ER-41320, and No. DE-SC0014552 and by the National Science Foundation under Grant No. PHY-0606007 and by the COPIN and COPIGAL French-Polish scientific exchange programs. K.W.B. was supported by a National Science Foundation Graduate Fellowship under Grant No. DGE-1143954 and J.M. was supported by a Department of Energy National Nuclear Security Administration Stewardship Science Graduate Fellowship under cooperative Agreement Number DE-NA0002135.

[1] A M Lane, "Studies in intermediate coupling iv: Further remarks on the nuclei ^{13}C and ^{13}N," Proceedings of the Physical Society. Section A **68**, 197 (1955).

[2] Dieter Kurath, "Intermediate coupling in the 1p-shell," Phys. Rev. **101**, 216–224 (1956).

[3] C. Mahaux, *Shell Model Approach to Nuclear Reactions* (North Holland, Amsterdam, 1969).

[4] H.W. Barz, I. Rotter, and J. Höhn, "Coupled channels calculations in the continuum shell model with complicated configurations," Nucl. Phys. A **275**, 111 – 140 (1977).

[5] K. Bennaceur, F. Nowacki, J. Okolowicz, and M. Ploszajczak, "Study of the ^{7}Be(p, γ)^{8}B and ^{7}Li(n, γ)^{8}Li capture reactions using the shell model embedded in the continuum," Nucl. Phys. A **651**, 289 – 319 (1999).

[6] J. Rotureau, J. Okołowicz, and M. Płoszajczak, "Theory of the two-proton radioactivity in the continuum shell model," Nucl. Phys. A **767**, 13 (2006).

[7] N. Michel, W. Nazarewicz, M. Płoszajczak, and K. Bennaceur, "Gamow shell model description of neutron-rich nuclei," Phys. Rev. Lett. **89**, 042502 (2002).

[8] R. Id Betan, R. J. Liotta, N. Sandulescu, and T. Vertse, "Two-particle resonant states in a many-body mean field," Phys. Rev. Lett. **89**, 042501 (2002).

[9] N Michel, W Nazarewicz, M Płoszajczak, and T Vertse, "Shell model in the complex energy plane," J. Phys. G **36**, 013101 (2009).

[10] J. Okołowicz, M. Płoszajczak, and I. Rotter, "Dynamics of quantum systems embedded in a continuum," Phys. Rep. **374**, 271 (2003).

[11] R. J. Charity, J. M. Elson, J. Manfredi, R. Shane, L. G. Sobotka, Z. Chajecki, D. Coupland, H. Iwasaki, M. Kilburn, Jenny Lee, W. G. Lynch, A. Sanetullaev, M. B. Tsang, J. Winkelbauer, M. Youngs, S. T. Marley, D. V. Shetty, and A. H. Wuosmaa, "Spin alignment of excited projectiles due to target spin-flip interactions," Phys. Rev. C **91**, 024610 (2015).

[12] D. E. M. Hoff, R. J. Charity, K. W. Brown, C. D. Pruitt, L. G. Sobotka, T. B. Webb, G. Potel, B. Roeder, and A. Saastamoinen, "Large longitudinal spin alignment of excited projectiles in intermediate energy inelastic scattering," Phys. Rev. Lett. **119**, 232501 (2017).

[13] B. Blank and M. Płoszajczak, "Two-proton radioactivity," Reports on Progress in Physics **71**, 046301 (2008).

[14] M. Pfützner, M. Karny, L. V. Grigorenko, and K. Riisager, "Radioactive decays at limits of nuclear stability," Rev. Mod. Phys. **84**, 567 (2012).

[15] G. J. Kunde, J. Pochodzalla, E. Berdermann, B. Berthier, C. Cerruti, C. K. Gelbke, J. Hubele, P. Kreutz, S. Leray, R. Lucas, U. Lynen, U. Milkau, C. Ngô, C. H. Pinkenburg, G. Raciti, H. Sann, and W. Trautmann, "Proton-proton correlations in ^{40}Ar+^{197}Au reactions and the role of the two-particle phase space," Phys. Rev. Lett. **70**, 2545 (1993).

[16] E. Cornell, T. M. Hamilton, D. Fox, Y. Lou, R. T. de Souza, M. J. Huang, W. C. Hsi, C. Schwarz, C. Williams, D. R. Bowman, J. Dinius, C. K. Gelbke, T. Glasmacher, D. O. Handzy, M. A. Lisa, W. G. Lynch, G. F. Peaslee, L. Phair, M. B. Tsang, G. VanBuren, R. J. Charity, L. G. Sobotka, and W. A. Friedman, "Assessing the evolutionary nature of multifragment decay," Phys. Rev. Lett. **75**, 1475 (1995).

[17] C. Schwarz, S. Fritz, R. Bassini, M. Begemann-Blaich, S.J. Gaff-Ejakov, D. Gourio, C. Groß, G. Immzé, I. Iori, U. Kleinevoß, G.J. Kunde, W.D. Kunze, U. Lynen, V. Maddalena, M. Mahi, T. Möhlenkamp, A. Moroni, W.F.J. Müller, G. Nociforo, B. Ocker, T. Ohed, F. Pertruzzelli, J. Pochodzalla, G. Raciti, G. Riccobene, F.P. Romano, A. Saija, M. Schnittker, A. Schttauf, W. Seidel, V. Serfling, C. Sfienti, W. Trautmann, A. Trzcinski, G. Verde, A. Wörner, Hongfei Xi, and B. Zwieglinski, "Time scales in spectator fragmentation," Nucl. Phys. A **681**, 279 (2001), 3rd Catania Relativistic Ion Studies.

[18] K. W. Brown, R. J. Charity, J. M. Elson, W. Reviol, L. G. Sobotka, W. W. Buhro, Z. Chajecki, W. G. Lynch, J. Manfredi, R. Shane, R. H. Showalter, M. B. Tsang, D. Weisshaar, J. R. Winkelbauer, S. Bedoor, and A. H. Wuosmaa, "Proton-decaying states in light nuclei and the first observation of ^{17}Na," Phys. Rev. C **95**, 044326 (2017).

[19] K. W. Brown, R. J. Charity, L. G. Sobotka, Z. Chajecki, L. V. Grigorenko, I. A. Egorova, Yu. L. Parfenova, M. V. Zhukov, S. Bedoor, W. W. Buhro, J. M. Elson, W. G. Lynch, J. Manfredi, D. G. McNeel, W. Reviol, R. Shane, R. H. Showalter, M. B. Tsang, J. R. Winkelbauer, and A. H. Wuosmaa, "Observation of long-range three-body coulomb effects in the decay of ^{16}Ne," Phys. Rev. Lett. **113**, 232501 (2014).

[20] K. W. Brown, R. J. Charity, L. G. Sobotka, L. V. Grigorenko, T. A. Golubkova, S. Bedoor, W. W. Buhro, Z. Chajecki, J. M. Elson, W. G. Lynch, J. Manfredi, D. G. McNeel, W. Reviol, R. Shane, R. H. Showalter, M. B. Tsang, J. R. Winkelbauer, and A. H. Wuosmaa, "Interplay between sequential and prompt two-proton decay from the first excited state of ^{16}Ne," Phys. Rev. C **92**, 034329 (2015).

[21] M. S. Wallace, M. A. Famiano, M.-J. van Goethem, A. M. Rogers, W. G. Lynch, J. Clifford, F. Delaunay, J. Lee, S. Labostov, M. Mocko, L. Morris, A. Moroni, B. E. Nett, D. J. Oostdyk, R. Krishnasamy, M. B. Tsang, R. T. de Souza, S. Hudan, L. G. Sobotka, R. J. Charity, J. Elson, and G. L. Engel, "The high resolution array (HiRA) for rare isotope beam experiments," Nucl. Instrum. Methods Phys. Res. A **583**, 302 (2007).

[22] M. J. Chromik, P. G. Thirolf, M. Thoennessen, B. A. Brown, T. Davinson, D. Gassmann, P. Heckman, J. Prisciandaro, P. Reiter, E. Tryggestad, and P. J. Woods, "Two-proton spectroscopy of low-lying states in ^{17}Ne," Phys. Rev. C **66**, 024313 (2002).

[23] A. M. Lane and R. G. Thomas, "R-matrix theory of nuclear reactions," Rev. Mod. Phys. **30**, 257 (1958).

[24] W.J. Huang, G. Audi, Meng Wang, F.G. Kondev, S. Naimi, and Xing Xu, "The AME2016 atomic mass evaluation (i). Evaluation of input data; and adjustment procedures," Chin. Phys. C **41**, 030002 (2017).

[25] K. Bennaceur, F. Nowacki, J. Okołowicz, and M. Płoszajczak, "Analysis of the ^{16}O(p,γ)^{17}F capture reaction using the shell model embedded in the continuum," Nucl. Phys. A **671**, 203 (2000).

[26] J. Okołowicz, M. Płoszajczak, and W. Nazarewicz, "On the origin of nuclear clustering," Prog. of Theor. Phys.

Supplement **196**, 230 (2012).
[27] J. Okołowicz, W. Nazarewicz, and M. Płoszajczak, "Towards understanding the microscopic origin of nuclear clustering," Fortschr. Phys. **61**, 66 (2013).
[28] A. Volya and V. Zelevinsky, "Continuum shell model," Phys. Rev. C **74**, 064314 (2006).
[29] C. Yuan, "Impact of off-diagonal cross-shell interaction on ^{14}C," Chin. Phys. C **41**, 104102 (2017).
[30] C. D. Zafiratos, F. Ajzenberg-Selove, and F. S. Dietrich, "$N^{14}(He^3, n)F^{16}$ reaction," Phys. Rev. **137**, B1479 (1965).
[31] T. Otsubo, I. Asada, M. Takeda, M. Tsuda, and Y. Oda, "Low-lying states of the ^{16}F nucleus," Nucl. Phys. A **259**, 452 (1976).
[32] D. W. Lee, K. Peräjärvi, J. Powell, J. P. O'Neil, D. M. Moltz, V. Z. Goldberg, and J. Cerny, "Low-lying resonant states in ^{16}F using a ^{15}O radioactive ion beam," Phys. Rev. C **76**, 024314 (2007).
[33] H. Fujita, G. P. A. Berg, Y. Fujita, J. Rapaport, T. Adachi, N. T. Botha, H. Fujimura, K. Fujita, K. Hara, K. Hatanaka, J. Kamiya, T. Kawabata, K. Nakanishi, R. Neveling, N. Sakamoto, Y. Sakemi, Y. Shimbara, Y. Shimizu, F. D. Smit, M. Uchida, T. Wakasa, M. Yoshifuku, M. Yosoi, and R. G. T. Zegers, "High resolution study of isovector negative parity states in the $^{16}O(^3He, t)^{16}F$ reaction at 140 MeV/nucleon," Phys. Rev. C **79**, 024314 (2009).
[34] I. Stefan, F. de Oliveira Santos, O. Sorlin, T. Davinson, M. Lewitowicz, G. Dumitru, J. C. Angélique, M. Angélique, E. Berthoumieux, C. Borcea, R. Borcea, A. Buta, J. M. Daugas, F. de Grancey, M. Fadil, S. Grévy, J. Kiener, A. Lefebvre-Schuhl, M. Lenhardt, J. Mrazek, F. Negoita, D. Pantelica, M. G. Pellegriti, L. Perrot, M. Płoszajczak, O. Roig, M. G. Saint Laurent, I. Ray, M. Stanoiu, C. Stodel, V. Tatischeff, and J. C. Thomas, "Probing nuclear forces beyond the drip-line using the mirror nuclei ^{16}N and ^{16}F," Phys. Rev. C **90**, 014307 (2014).
[35] J. Okołowicz, M. Płoszajczak, and Y. Luo, "Continuum coupling effects in spectra of mirror nuclei and binding systematics," Acta Phys. Pol. B **39**, 389 (2008).